Abdominal Radiology

Published online: 9 July 2018

Abdom Radiol (2019) 44:180–189
https://doi.org/10.1007/s00261-018-1688-8

Association of qualitative and quantitative imaging features on multiphasic multidetector CT with tumor grade in clear cell renal cell carcinoma

Heidi Coy,[1] Jonathan R. Young,[2] Michael L. Douek,[1] Alan Pantuck,[3] Matthew S. Brown,[1] James Sayre,[4] and Steven S. Raman[5]

[1]Department of Radiological Sciences, David Geffen School of Medicine at UCLA, Ronald Reagan-UCLA Medical Center, 924 Westwood Boulevard, Suite 650, Los Angeles, CA 90024, USA
[2]Department of Radiology, University of California, Davis, 4860 Y Street, Suite 3100, Sacramento, CA 95817, USA
[3]Department of Urology, David Geffen School of Medicine at UCLA, Ronald Reagan-UCLA Medical Center, Clark Urology Center-Westwood, 200 Medical Plaza, Suite 140, Los Angeles, CA 90095, USA
[4]Department of Biostatistics, UCLA School of Public Heath, Room 51-253A, Los Angeles, CA 90095, USA
[5]UCLA Department of Radiological Sciences, Ronald Reagan UCLA Medical Center, 757 Westwood Plaza, RRUMC 1621H, Box 957437, Los Angeles, CA 90095, USA

Abstract

Purpose: The purpose of the study was to determine if enhancement features and qualitative imaging features on multiphasic multidetector computed tomography (MDCT) were associated with tumor grade in patients with clear cell renal cell carcinoma (ccRCC).

Methods: In this retrospective, IRB approved, HIPAA-compliant, institutional review board-approved study with waiver of informed consent, 127 consecutive patients with 89 low grade (LG) and 43 high grade (HG) ccRCCs underwent preoperative four-phase MDCT in unenhanced (UN), corticomedullary (CM), nephrographic (NP), and excretory (EX) phases. Previously published quantitative (absolute peak lesion enhancement, absolute peak lesion enhancement relative to normal enhancing renal cortex, 3D whole lesion enhancement and the wash-in/wash-out of enhancement within the 3D whole lesion ROI) and qualitative (enhancement pattern; presence of necrosis; pattern of; tumor margin; tumor–parenchymal interface, tumor–parenchymal interaction; intratumoral vascularity; collecting system infiltration; renal vein invasion; and calcification) assessments were obtained for each lesion independently by two fellowship-trained genitourinary radiologists. Comparisons between variables included χ^2, ANOVA, and student t test. p values less than 0.05 were considered to be significant. Inter-reader agreement was obtained with the Gwet agreement coefficient (AC1) and standard error (SE) was reported.

Results: No significant differences were observed between the LG and HG ccRCC cohorts with respect to absolute peak lesion enhancement and relative lesion enhancement ratio. There was a significant inverse correlation between low and high grade ccRCC and tumor enhancement the NP (71 HU vs. 54 HU, $p < 0.001$) and EX (52 HU vs. 39 HU, $p < 0.001$) phases using the 3D whole lesion ROI method. The percent wash-in of 3D enhancement from the UN to the CM phase was also significantly different between LG and HG ccRCCs (352% vs. 255%, $p = 0.003$). HG lesions showed significantly more calcification, necrosis, collecting system infiltration and ill-defined tumor margins ($p < 0.05$). Overall agreement between the two readers had a mean AC1 of 0.8172 (SE 0.0235).

Conclusions: Quantitatively, high grade ccRCC had significantly lower whole lesion enhancement in the NP and EX phases on MDCT. Qualitatively, high grade ccRCC were significantly more likely to be associated

Correspondence to: Heidi Coy; *email:* hcoy@mednet.ucla.edu

with calcifications, necrosis, collecting system infiltration, and an ill-defined tumor margin.

Key words: Clear cell renal cell carcinoma—Fuhrman nuclear grade—Renal computed tomography—Neoplasm grading—Kidney—Tumor heterogenity

The incidence of renal cell carcinoma (RCC) is increasing 2% annually and has increased 30% globally since 1990 [1]. Previous studies have investigated how to best differentiate patients with low and high risk RCC, and several risk scores based on clinical features of RCC including stage, size, grade, and histological subtype have been identified and clinically validated [2]. Clear cell renal cell carcinoma (ccRCC) comprises ~ 90% of all RCC and has the worst prognosis and highest metastatic potential [3]. The Fuhrman grading system and more recently, the International Society of Urological Pathology (ISUP), have stratified ccRCC tumors into four grades based on nuclear morphology [4, 5]. Pre-treatment percutaneous core biopsy of renal masses is becoming widely adopted for diagnosis of histology and to a lesser extent, tumor grade, to determine a treatment plan. However, biopsy is more accurate for determining histology (86–98%) than tumor grade (46–64%) and can be discordant with surgical pathology [6–10] due in part to the inherent genetic heterogeneity of ccRCC [11].

As 70% of renal masses are characterized incidentally on routine clinical imaging, a noninvasive method to determine tumor grade on imaging may be of clinical value [6]. Previous studies have investigated the association quantitative enhancement features and qualitative assessment on multidetector multiphasic CT (MDCT) and magnetic resonance imaging (MRI) with clinical endpoints including tumor grade, histology, survival outcomes, and treatment response [12–22].

Compared to biopsy and immunohistochemistry, MDCT is noninvasive and widely used in routine clinical practice for detection, characterization, and staging of renal masses. An imaging-based method to predict tumor grade may guide clinical triage in incidentally detected ccRCC to active surveillance, percutaneous thermal ablation or surgical intervention with or without adjuvant, or even neoadjuvant, targeted antiangiogenic therapies [4, 23–25]. The primary aim of this study was to assess if quantitative enhancement features and qualitative assessment on multiphasic MDCT were associated with tumor grade in patients with ccRCC.

Methods

In a prior study [26], we reported on 78 (61%) of the patients included in our current cohort. However, the prior study examined the utility of a computer-aided diagnostic algorithm (CAD) to determine peak lesion enhancement and discriminate the ccRCC histological subtype from more indolent RCC subtypes and benign renal masses, and also compared the performance of the CAD algorithm to that of a radiologist. Our current analysis focuses on the utility of noninvasively discriminating tumor grade in patients with ccRCC from routine clinical images. Therefore, we only reviewed the cohort of patients with the ccRCC histological subtype, while expanding upon our prior work by including a larger patient population. We also investigated the utility of four different quantitative enhancement features in combination with qualitative features to predict tumor grade in patients with ccRCC.

Study population

Figure 1 portrays the subject accrual flowchart. We retrospectively queried our institution's pathology, imaging and clinical databases for consecutive patients who had undergone surgical resection or biopsy of ccRCC between January 2000 and January 2016. Patients were eligible for inclusion if they underwent a preoperative MDCT with a four-phase renal mass protocol and had a histologically proven ccRCC with a diagnosis of Fuhrman grade I to IV. The initial query yielded a target population of 178 consecutive patients who were considered eligible for inclusion in the study. Subjects were considered ineligible for this study if (a) the ccRCC was a metastatic lesion, (b) the histological diagnosis was mixed, (c) the image quality was deemed inadequate due to suboptimal injection technique or poor timing of the post-contrast phases, (d) the tumor tissue sample was inadequate for immunohistochemistry. Of the 178 patients who were deemed initially eligible for the study, 51 were excluded from our target population for one or more of these indications.

Our final study cohort comprised 127 consecutive patients [mean age, 62 years, ± 14.8 (standard deviation)]; range 22–91 years, including 81 men (mean age, 61 years, ± 13.7; age range 27–91 years) and 46 women (mean age, 63 years, ± 16.5; age range 22–87 years) with a total of 132 ccRCC lesions. Three of the patients had two lesions each. Mean time from MDCT to surgery or biopsy for all patients was 61 days (range 0–407 days).

Four-phase renal mass CT protocol

All patients had a preoperative MDCT at our institution with an intravenous contrast-enhanced four-phase renal mass protocol. Our scans of the abdomen included an unenhanced (UN) scan and contrast-enhanced acquisitions during the corticomedullary (CM), nephrographic (NP), and excretory (EX) phases acquired from the lung bases to the iliac crests. Preoperative MDCT was performed on multiple scanners (4-MDCT, 16-MDCT, and

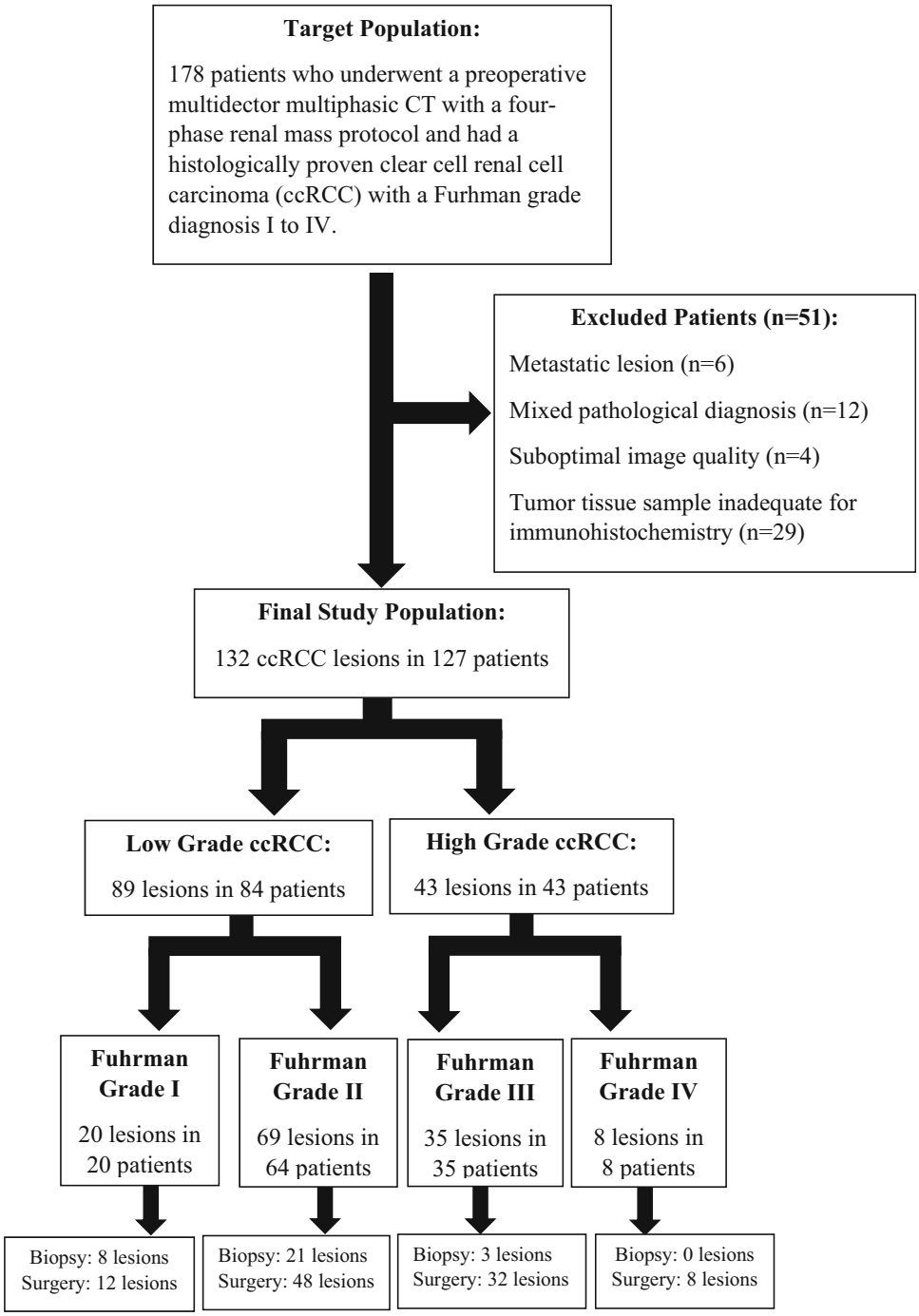

Fig. 1. Flowchart shows selection of study population.

64-MDCT). Acquisition parameters were similar over the multiple generations of scanners: 120 KVp, 200–400 mA based on patient size and 3-mm scan collimation with 3-mm reconstruction intervals. No difficulties were observed in assessing patients scanned on earlier generation (4- and 16-MDCT) helical scanners due to similar slice thickness acquisition.

Patients received a power injection of nonionic IV contrast material (iodixanol, Omnipaque 350, GE Healthcare), 35–45 g iodine dosed to weight at a rate of 3 mL/s. Patients who weighed less than 45 kg, those who weighed 45–90 kg, and those who weighed $>$ 90 kg received 100 mL (35 g iodine), 125 mL (45 g iodine), and 150 mL (54 g iodine) of contrast material, respectively. A bolus tracking system (Care Bolus VB10, Siemens Healthcare or Smart-Prep, GE Healthcare) was used to determine the onset of imaging and a region of interest (ROI) was placed in the thoracoabdominal aorta junc-

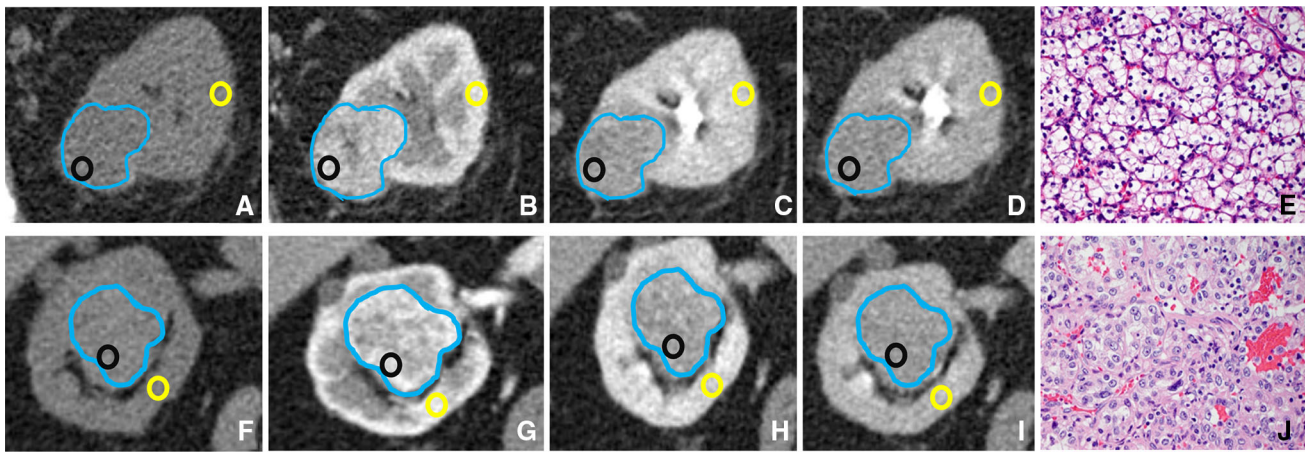

Fig. 2. Example of quantitative enhancement measurements and pathological assessment from a 61-year-old man with pathologically proven 3.5-cm low grade clear cell renal cell carcinoma (Fuhrman grade II) (**A**–**E**) and from an 85-year-old man with pathologically proven 3.6-cm high grade clear cell renal cell carcinoma (Fuhrman grade IV) (**F**–**J**). **A**–**D**, **F**–**J** One circular ROI with a 0.5 cm diameter was manually selected in the maximally enhancing portion of solid tumor in each imaging phase (black ROI) in the axial plane to calculate the absolute peak lesion enhancement (red ROI). A second ROI was placed in uninvolved renal cortex (yellow ROI) to calculate tumor enhancement ratio. The entire tumor volume was manually contoured in the axial plane in each of the four phases (blue ROI) resulting in a 3D ROI representative of the entire lesion. The 3D lesion contours were used to calculate the mean absolute 3D tumor volume enhancement and the wash-in and wash-out of enhancement within the lesion. **E**, **J** Hematoxylin and eosin staining shows slightly irregular nuclei, nuclear diameter of 15 microns and open chromatin indicative of a low grade clear cell renal cell carcinoma (**E**) and mitoses, multilobulated pleomorphic cells and macronuclei indicative of a high grade clear cell renal cell carcinoma (**J**).

tion, with a trigger set to begin at 150 HU. Images were acquired at 55 s (CM), 120 s (NP), and 8 min (EX) after the threshold of 150 HU was reached. For the patients imaged with earlier generation (4- and 16-MDCT) helical scanners, the CM and NP phases were performed slightly earlier (40 and 50 s and 90 and 110 seconds after the threshold of 150 HU was reached, respectively). Overall, there was very little variation in the timing of image acquisition: all included patients were imaged within 5 s of stated times.

Quantitative image analysis

Quantitative image analysis was initially performed by one research associate with six years of experience in abdominal CT image analysis (HC) and one first year radiology attending (JRY). All ROIs and tumor contours were confirmed for appropriate placement by two fellowship trained genitourinary abdominal radiologists with 21 (SSR) and 11 (MLD) years of experience who were blinded to all patient information, including the pathological diagnosis. Cases where the radiologists disagreed were resolved by consensus.

Four quantitative enhancement measures that have been shown to correlate with tumor grade and other clinical endpoints in RCC [17–21, 26–29] were obtained for each patient's pathologically proven lesion. First, to compare absolute peak ccRCC enhancement, data were obtained by manually selecting one circular ROI with a 0.5 cm diameter in the maximally enhancing portion of solid tumor by visual inspection in each imaging phase. Using the co-registration tool on PACS and anatomic landmarks for guidance, one circular ROI with a 0.5 cm diameter representative of peak lesion enhancement was placed in the same location on each of the four imaging phases in the axial plane. Areas of calcification and artifact were avoided. Absolute peak lesion enhancement in each post-contrast phase was calculated as post-contrast phase of enhancement (HU)-unenhanced phase (HU) [17–21, 26] (Fig. 2A–D, F–I).

Second, to normalize for variation in attenuation due to individual patient and technical factors, another circular ROI was placed in uninvolved renal cortex and the relative tumor enhancement ratio was calculated as follows: (tumor enhancement in the post-contrast phase-tumor in unenhanced phase)/(cortex enhancement in the post-contrast phase-cortex in the unenhanced phase) [26, 27] (Fig. 2A–D, F–I).

Third, to account for tumor heterogeneity, the entire tumor volume was manually contoured in the axial plane in each of the four phases using a DICOM-based FDA approved in-house image processing software. Tumor segmentation was limited to the target tumor and included regions of solid tumor, gross necrosis, fibrosis, and hemorrhage within the 3D ROI, and excluded normal renal parenchyma, renal sinus or adjacent perirenal

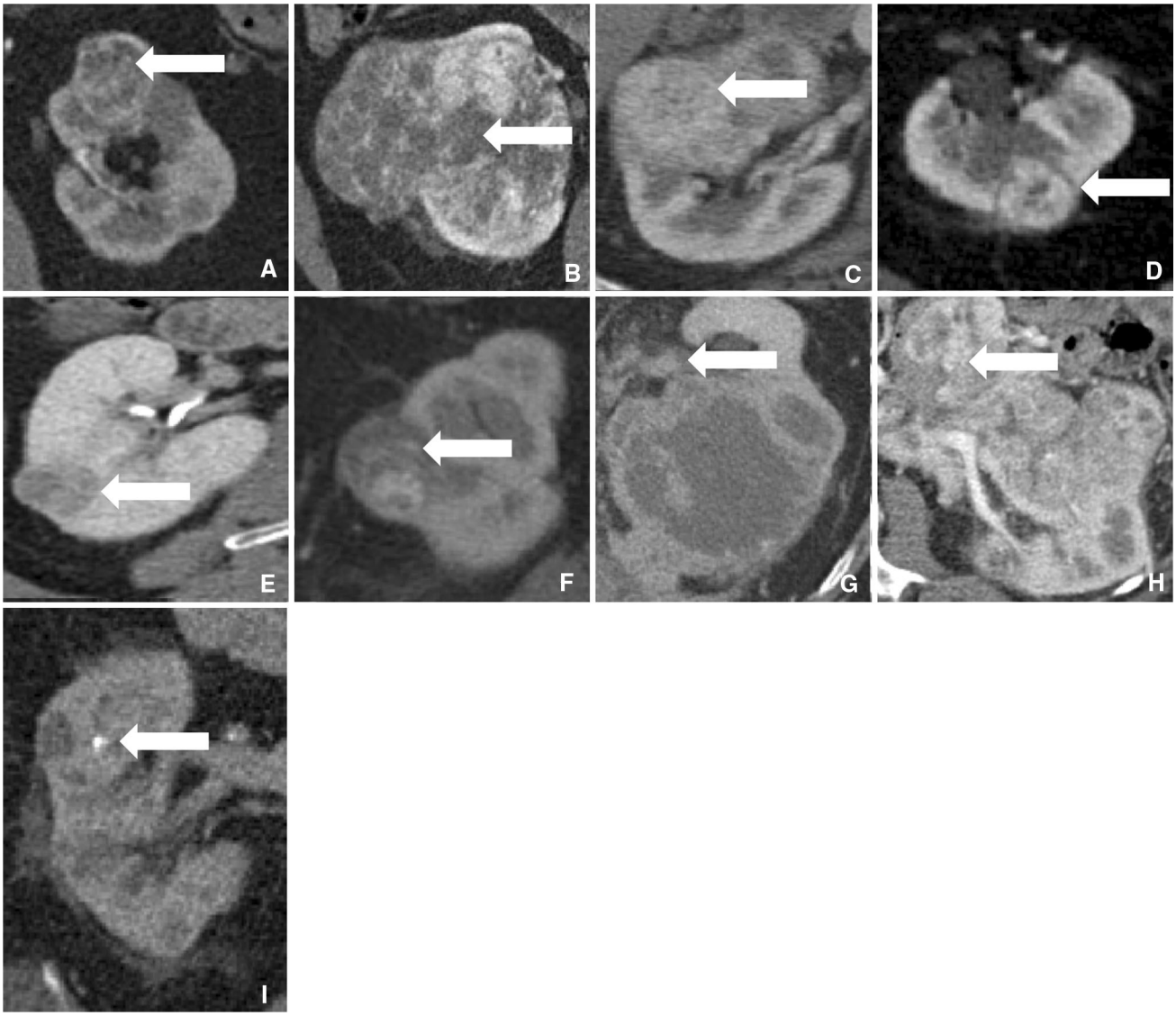

Fig. 3. Illustration of qualitative CT features of clear cell renal cell carcinoma investigated in this study: (**A**) Enhancement pattern, (**B**) Presence of necrosis and pattern of necrosis, (**C**) Tumor margin, (**D**) Tumor–parenchymal interface, (**E**) Tumor–parenchymal interaction, (**F**) Intratumoral vascularity, (**G**) Collecting system infiltration, (**H**) Renal vein invasion, (**I**) Calcification. Arrow indicates feature of interest in each image.

fat. The 3D volume was used as the ROI to calculate mean enhancement of the entire tumor in each post-contrast phase using the formula: 3D lesion enhancement in the post-contrast phase (HU)-3D lesion UN phase (HU) [28]. Fourth, to further investigate enhancement patterns of the tumor on multiphasic MDCT, the wash-in and wash-out of enhancement within the 3D ROI was calculated using a CT wash-out formula developed by Kopp et al. [29] (Fig 2A–D, F–I)

Qualitative imaging features

CT examinations were reviewed independently by two abdominal fellowship-trained genitourinary radiologists with 21 (SSR) and 11 (MLD) years of experience. Both readers were blinded to all clinical, pathologic, and imaging findings. Cases where the radiologists disagreed were resolved by consensus. They evaluated each ccRCC lesion for each of the previously published features [12]: enhancement pattern (homogeneous vs. heterogeneous); presence of necrosis; pattern of necrosis (percentage of tumor volume that is necrotic: 0–25%, 26–50%, 51–75%, or 76–100%); tumor margin (well-defined vs. ill-defined); tumor–parenchymal interface (presence of a hypoattenuating rim completely or partially circumscribing the tumor on delayed phase imaging), tumor–parenchymal interaction (presence of a discrete rim of enhancement partially or completely circumscribing the tumor on de-

layed phase imaging in the absence of a hypoattenuating rim); intratumoral vascularity; collecting system infiltration; renal vein invasion; and calcification (Fig. 3).

Clinical reference standard

Histopathologic analysis and Fuhrman grade assignment after nephrectomy or biopsy served as the reference standard for all tumors (Fig. 2E, J). Prior studies have shown that intra- and interobserver agreement among pathologists is improved when the Fuhrman grading system is collapsed into two categories [30]. Therefore, ccRCC lesions with Fuhrman grades I and II were categorized as low grade (LG) and ccRCC lesions with Fuhrman grades III and IV were categorized as high grade (HG).

Statistical analysis

Continuous variables were analyzed by Student *t* test and ANOVA. Categorical variables were analyzed by χ^2 test. *p* values less than 0.05 were considered to be statistically significant. Inter-reader agreement was obtained with the Gwet agreement coefficient (AC1) and standard error (SE) were reported. Statistical analysis was performed with SPSS software (version 20.0, IBM SPSS).

Results

Patient and lesion characteristics

Table 1 describes the clinicopathologic characteristics of the entire cohort. We analyzed 84 patients with 89 LG ccRCCs and 43 patients with 43 HG ccRCCs. The HG ccRCCs were significantly larger than LG ccRCCs (mean lesion size 5.3 vs. 3.1 cm, $p < 0.001$), respectively.

Quantitative MDCT enhancement measures

No significant differences were observed between the LG and HG ccRCC cohorts with respect to peak lesion enhancement and relative lesion enhancement ratio in all of the post-contrast phases (Table 2, Figs. 4, 5). There was a significant inverse correlation between LG and HG ccRCCs in the 3D lesion enhancement values the NP (71 HU vs. 54 HU, $p < 0.001$) and EX (52 HU vs. 39 HU, $p < 0.001$) phases with no overlap

Table 1. Patient demographics and clinical features

Characteristic	Statistic	All clear cell renal cell carcinomas *n* = 132	Low grade clear cell renal cell carcinomas (Fuhrman grades I and II) *n* = 89	High grade clear cell renal cell carcinomas (Fuhrman grades III and IV) *n* = 43
Gender				
Male	*n* (%)	81(64)	52 (61)	29 (69)
Female	*n* (%)	46 (36)	33 (39)	13 (31)
Age at diagnosis (year)	Mean (range)	61 (22–91)	60 (22–91)	63 (37–85)
Laterality of tumor				
Right kidney	*n* (%)	60 (45)	42 (47)	18 (42)
Left kidney	*n* (%)	72 (55)	47 (53)	25 (58)
Tumor size (cm)	Mean (range)	3.9 (0.8–16.1)	3.1 (0.8–11.2)	5.5 (1.0–16.1)*
Fuhrman grade				
I	*n* (%)	20 (15)	89 (67)	–
II	*n* (%)	69 (52)		
III	*n* (%)	35 (27)	–	43 (33)
IV	*n* (%)	8 (6)		
T stage				
T1a	*n* (%)	76 (56)	66 (74)	10 (23)
T1b	*n* (%)	27 (21)	15 (17)	12 (28)
T2a	*n* (%)	5 (4)	2 (3)	3 (7)
T2b	*n* (%)	1 (1)	1 (1)	0 (0)
T3a	*n* (%)	14 (11)	2 (2)	12 (28)
T3b	*n* (%)	9 (7)	3 (3)	6 (14)
T4	*n* (%)	0 (0)	0 (0)	0 (0)
Time from 4-phase MDCT to specimen acquisition (days)	Mean (range)	61 (0–407)	70 (0–367)	63 (0–407)
Method of specimen acquisition				
Biopsy	*n* (%)	32 (24)	29 (33)	3 (7)
Partial nephrectomy	*n* (%)	59 (45)	40 (45)	19 (44)
Total nephrectomy	*n* (%)	22 (17)	16 (18)	6 (14)
Radical nephrectomy	*n* (%)	19 (14)	4 (4)	15 (35)

SD, Standard deviation; MDCT, multidetector computed tomography
*Statistically significant vs. low grade cohort ($p < 0.05$)

Table 2. Quantitative enhancement characteristics of low and high grade clear cell renal cell carcinomas

Enhancement characteristic	Low grade $n = 89$	High grade $n = 43$	p value
Absolute peak lesion enhancement (HU)			
Unenhanced phase	31.1 (29.3–33.0)	31.4 (29.3–33.5)	0.856
Corticomedullary phase	152.3 (141.4–163.1)	165.2 (149.0–181.5)	0.198
Nephrographic phase	110.5 (104.0–117.0)	107.6 (100.8–114.5)	0.556
Excretory phase	86.7 (82.1–91.3)	84.8 (78.3–91.3)	0.636
Relative tumor enhancement ratio			
Corticomedullary phase	1.3 (1.0–1.6)	1.2 (0.9–1.6)	0.792
Nephrographic phase	0.6 (0.5–0.7)	0.7 (0.6–0.8)	0.237
Excretory phase	0.7 (0.6–0.7)	0.7 (0.6–0.8)	0.506
3D tumor volume enhancement (HU)			
Unenhanced phase	24.7 (23.4–26.1)	28.2 (25.9–30.5)	0.012*
Corticomedullary phase	79.1 (71.8–86.4)	66.9 (56.4–77.3)	0.064
Nephrographic phase	71.3 (66.4–76.1)	53.7 (47.1–60.2)	< 0.001*
Excretory phase	52.4 (48.6–56.2)	39.1 (34.6–43.6)	< 0.001*
3D tumor volume enhancement wash-in and wash-out (%)			
Wash-in (unenhanced to corticomedullary)	352.2 (309.5–395.0)	254.6 (208.9–300.3)	0.003*
Wash-out (corticomedullary to nephrographic)	14.4 (5.5–23.3)	22.5 (9.8–35.3)	0.309
Wash-out (nephrographic to excretory)	39.3 (33.8–44.9)	40.8 (30.9–50.7)	0.795

Data are the mean and 95% CI of the mean in parentheses
*Statistically significant vs. low grade cohort ($p < 0.05$)

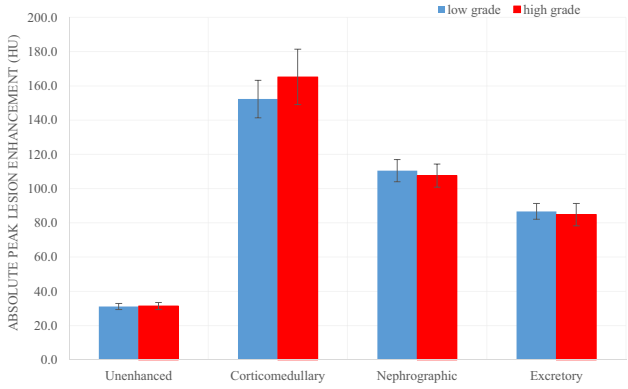

MDCT=Multidetector computed tomography. HU=Hounsfield unit.

Fig. 4. Bar graph shows absolute peak lesion enhancement in each post-contrast phase on MDCT for low and high grade clear cell renal cell carcinomas. Data points are mean peak lesion enhancement (HU) in the unenhanced phase and in each post-contrast phase. Error bars = 95% CIs for the mean. MDCT, Multidetector computed tomography; HU, Hounsfield unit.

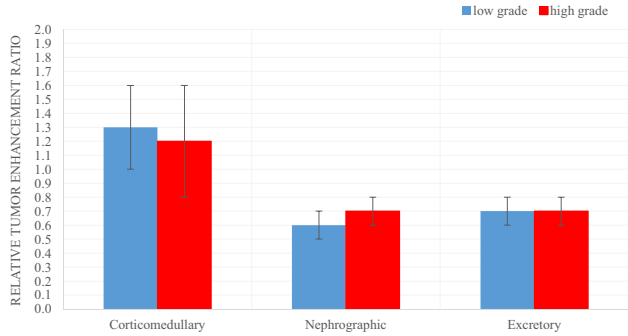

MDCT=Multidetector computed tomography.

Fig. 5. Bar graph shows relative tumor enhancement ratio in each post-contrast phase on MDCT for low and high grade clear cell renal cell carcinomas. Data points are mean relative tumor enhancement ratio in each post-contrast phase. Error bars = 95% CIs for the mean. MDCT, Multidetector computed tomography.

of the 95% CIs (Table 2, Fig. 6). The percent wash-in of 3D enhancement from the UN to the CM phase was also significantly different between LG and HG ccRCCs (352% vs. 255%, $p = 0.003$) (Table 2, Fig. 7).

Qualitative imaging features

The results for qualitative imaging features are described in Table 3. Four qualitative imaging features were significantly associated with HG ccRCC (calcification, necrosis, collecting system infiltration, and tumor margin) compared to LG RCC ($p < 0.05$). Overall agreement between the two readers for all qualitative features had a mean AC1 of 0.8172 (SE 0.0235).

Discussion

In this study, we investigated which quantitative enhancement measurements and qualitative imaging features on MDCT were associated with tumor grade in ccRCC. We found there was a significant inverse correlation between tumor grade and enhancement when we used a 3D ROI representative of the entire tumor to

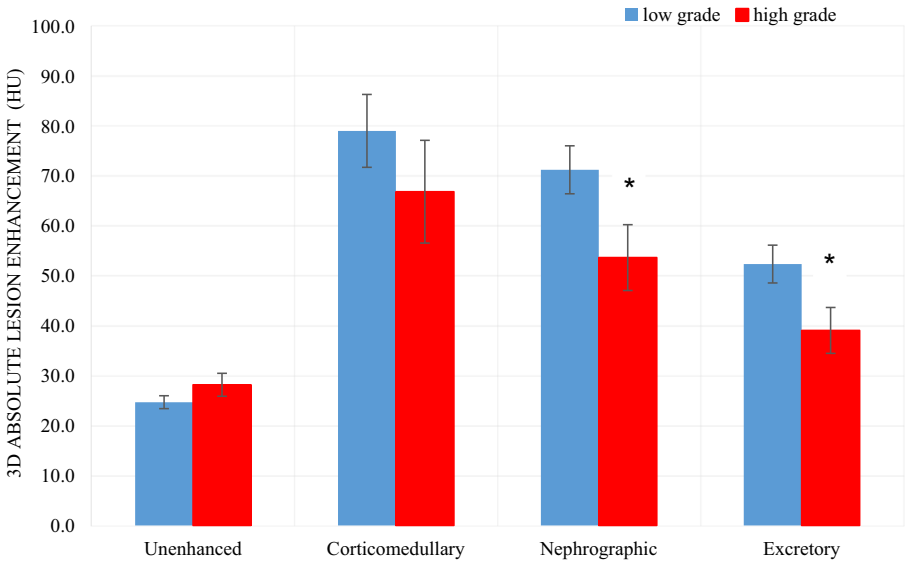

MDCT=Multidetector computed tomography. HU=Hounsfield unit.
*Statistically significant vs. low grade cohort (P<0.05).

Fig. 6. Bar graph shows 3D whole lesion enhancement in each phase on MDCT for low and high grade clear cell renal cell carcinomas. Data points are mean enhancement (HU) in each phase. Error bars = 95% CIs for the mean. MDCT, Multidetector computed tomography; HU, Hounsfield unit. *Statistically significant vs. low grade cohort ($P < 0.05$).

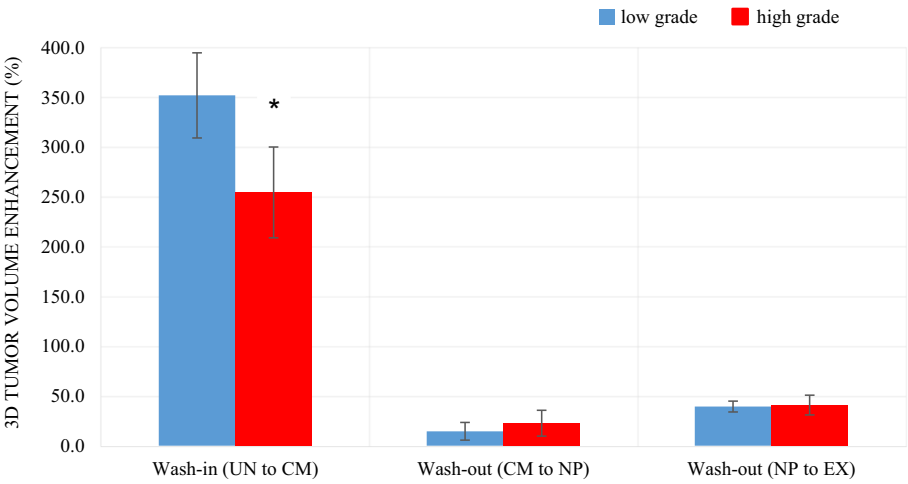

MDCT=Multidetector computed tomography.
*Statistically significant vs. low grade cohort (P<0.05).

Fig. 7. Bar graph shows wash-in and wash-out of enhancement derived from whole lesion 3D contours on MDCT for low and high grade clear cell renal cell carcinomas. Data points are mean percent wash-in and wash-out across each post-contrast phase acquired. Error bars = 95% CIs for the mean. MDCT = Multidetector computed tomography. *Statistically significant vs. low grade cohort ($P < 0.05$).

quantify enhancement in the NP and EX phases, with no overlap in the 95% CIs. In the CM phase, a static measure of 3D whole lesion enhancement only trended towards significance; however, we found when quantifying a dynamic change of the wash-in of enhancement, LG ccRCCs had a significantly higher wash-in of enhancement from the UN to the CM phase than the HG ccRCCs. Qualitative assessment of the lesions showed that HG ccRCCs were significantly associated with calcification, necrosis, collecting system infiltration, and an ill-defined tumor margin.

Given the established association between increased angiogenesis and tumor aggressiveness of the HG tumors, it may seem counterintuitive that a HG ccRCC

Table 3. Qualitative enhancement characteristics of low and high grade clear cell renal cell carcinomas

Qualitative imaging feature	Low grade $n = 89$	High grade $n = 43$	P value
Calcification			
Present	6 (7)	11 (26)	.0045*
Absent	83 (93)	32 (74)	
Enhancement pattern			
Homogeneous	15 (17)	4 (9)	.2994
Heterogeneous	74 (83)	39 (91)	
Presence of necrosis			
Present	44 (49)	30 (70)	.0391*
Absent	45 (51)	13 (30)	
Pattern of necrosis			
0–25%	73 (82)	28 (65)	.1373
26–50%	10 (11)	10 (23)	
51–75%	5 (6)	3 (7)	
76–100%	1 (1)	2 (5)	
Tumor margin			
Well-defined	81 (91)	30 (70)	.0041*
Ill-defined	8 (9)	13 (30)	
Tumor–parenchymal interface			
Present	7 (8)	2 (5)	.7173
Absent	82 (92)	41 (95)	
Tumor–parenchymal interaction			
Present	7 (8)	1 (2)	.7173
Absent	82 (92)	42 (98)	
Intratumoral vascularity			
Present	58 (65)	29 (67)	.8467
Absent	31 (35)	14 (33)	
Collecting system infiltration			
Present	2 (2)	6 (14)	.0146*
Absent	87 (98)	37 (86)	
Renal vein invasion			
Present	4 (4)	6 (14)	.0777
Absent	85 (96)	37 (86)	

Data are the number and percent in parentheses
*Statistically significant vs. low grade cohort ($p < 0.05$)

would have a lower mean whole lesion enhancement compared to a LG ccRCC. However, our qualitative assessment of the lesions may help to explain, in part, our results. We found that HG ccRCC had significantly more necrosis than LG ccRCC, which is concordant with previous studies which attempted to qualitatively assess clinical CT features to predict high grade ccRCCs [16, 31]. In addition, it is highly likely these ccRCCs also contained regions of histological necrosis, difficult to identify on MDCT [27]. These types of necrosis likely contribute to nonviable tissue within the tumor and prenecrotic hypovascularity as the tumor outgrows its blood supply [32].

Interestingly, when we used a small ROI in the most avidly enhancing portion of the tumor to quantify absolute peak lesion enhancement and relative enhancement ratio, we did not find a significant association using this method between enhancement and tumor grade. This is concordant with previous findings by Sun et al. and Vargas et al. However, when Villalobos-Gollas et al. [20] and Zhu et al. [27] quantified enhancement with either a single large 2D ROI or a limited number of small ROIs within the tumor on multiphasic MDCT they were able to significantly differentiate HG from LG ccRCCs. These differences may be due in part to sample size and differences in the timing acquisition of the scans, but also due to the inherent intra-observer variability associated with manual ROI placement [26]. It is also unlikely that a single ROI can be representative of the entire ccRCC due to its heterogeneous nature.

Huhdanpaa et al. [28] and Vargas et al. [33] showed that a 3D ROI representative of the entire lesion on MDCT and MRI can differentiate LG from HG ccRCCs in the NP and EX phases. Huhdanpaa et al. found that on MDCT, the IQR, standard deviation of enhancement in the NP phase, and absolute enhancement are significantly more heterogeneous for LG ccRCC and Vargas et al. found that on MRI, all significant associations between 3D enhancement and tumor grade were in the NP and EX phases. Our findings are concordant with these results and go a step further to show there is no overlap in the 95% CIs of the absolute mean enhancement values of LG and HG lesions in these two post-contrast phases, likely due to our increased sample size.

Our study had some potential limitations. First, since this was a proof of concept single-center retrospective study, and the results should be further validated on an independent cohort in a prospective trial. Second, the low number of Fuhrman grade I and IV tumors with preoperative 4-phase MDCT precluded a large number of these tumor types being included in our analysis. Third, we included three patients with two LG lesions each, which may have a small potential for clustering effects. Fourth, we included 25% of patients in whom tumor grade was determine by percutaneous core biopsy.

With an increased rate of RCC detection, a reliable means to characterize multiple aspects of ccRCC biology on imaging may provide a more robust noninvasive understanding of individual lesions possibly decreasing the need for more invasive procedures such as renal mass biopsy. While no single method provides insight into multiple aspects of renal tumor biology, our results indicate that a 3D ROI representative of the entire renal mass can provide objective quantitative data of enhancement changes within the tumor associated with tumor grade and MVD which can be used as part of a prognostic multiparametric model to suggest tumor grade in patients with ccRCC. Our method is easily translatable to clinical practice and can be applied to routine MDCT images to assist the clinician in triaging patients to the appropriate therapy.

Compliance with ethical standards

Conflict of interest All authors have no conflicts of interest.

Informed consent This retrospective, single-center, Health Insurance Portability and Accountability Act-compliant study was approved by the Institutional Review board and a waiver of informed consent was obtained.

References

1. Global Burden of Disease Cancer Collaboration (2015) The global burden of cancer 2013. JAMA Oncol 1:505–527
2. Lam JS, Shvarts O, Leppart JT, et al. (2005) Postoperative surveillance protocol for patients with localized and locally advanced renal cell carcinoma based on a validated prognostic nomogram and risk group stratification system. J Urol 174:466–472
3. Sun M, Shariat SF, Cheng C, et al. (2011) Prognostic factors and predictive models in renal cell carcinoma: a contemporary review. Eur Urol 60(4):644–661
4. Fuhrman SA, Lasky LC, Limas C (1982) Prognostic significance of morphologic parameters in renal cell carcinoma. Am J Surg Pathol 6(7):655–663
5. Delahunt B, Egevad L, Montironi R, et al. (2013) International Society of Urological Pathology (ISUP) consensus conference on renal neoplasia: rationale and organization. Am J Surg Pathol 37:1463–1468
6. Silverman SG, Israel GM, Trinh QD (2015) Incompletely characterized incidental renal masses: emerging data support conservative management. Radiology 275(1):28–42
7. Lebret T, Poulain JE, Molinie V, et al. (2007) Percutaneous core biopsy for renal masses: indications, accuracy and results. J Urol 178(4 Pt 1):1184–1188 (discussion 1188. 75)
8. Leveridge MJ, Finelli A, Kachura JR, et al. (2011) Outcomes of small renal mass needle core biopsy, nondiagnostic percutaneous biopsy, and the role of repeat biopsy. Eur Urol 60(3):578–584
9. Halverson SJ, Kunju LP, Bhalla R, et al. (2013) Accuracy of determining small renal mass management with risk stratified biopsies: confirmation by final pathology. J Urol 189(2):441–446
10. Ball MW, Bezerra SM, Gorin MA, et al. (2015) Grade heterogeneity in small renal masses: potential implications for renal mass biopsy. J Urol 193(1):36–40
11. Gerlinger Rowan, Horswell S, et al. (2012) Intratumor heterogeneity and branched evolution revealed by multiregion sequencing. N Engl J Med 366(10):883–892
12. Jamshidi N, Jonasch E, Zapala M, et al. (2015) The radiogenomic risk score: construction of a prognostic quantitative, noninvasive image-based molecular assay for renal cell carcinoma. Radiology 277:114–123
13. Lubner M, Stabo N, Abel EJ, Munoz del Rio A, Pickhardt PCT (2016) Textural analysis of large primary renal cell carcinomas: pretreatment tumor heterogeneity correlates with histologic findings and clinical outcomes. AJR 207:96–105
14. Yin Q, Hung SC, Wang L, et al. (2017) Associations between tumor vascularity, vascular endothelial growth factor expression and PET/MRI radiomic signatures in primary clear cell renal cell carcinoma: proof of concept study. Sci Rep 7:43356. https://doi.org/10.1038/srep43356
15. Shinagare A, Krajewski K, Braschi-Amirfarzan M, Ramaiya N (2017) Advanced renal cell carcinoma: role of the radiologist in the era of precision medicine. Radiology 284(2):333–351
16. Ishigami K, Leite L, Pakalniskis M, et al. (2014) Tumor grade of clear cell renal cell carcinoma assessed by contrast-enhanced computed tomomgraphy. SpringerPlus 3:694
17. Rosenkrantz AB, Niver BE, Fitzgerald EF, et al. (2010) Utility of the apparent diffusion coefficient for distinguishing clear cell renal cell carcinoma of low and high nuclear grade. Am J Roentgenol 195:W344–W351
18. Reiner C, Roessle M, Thiesler T, et al. (2013) Computed tomography perfusion imaging of renal cell carcinoma. Invest Radiol 48:183–191
19. Jinzaki M, Tanimoto A, Mukai M, et al. (2000) Double-phase helical CT of small renal parenchymal neoplasms: correlation with pathologic findings and tumor angiogenesis. J Comput Assist Tomogr 24(6):835–842
20. Villalobos-Gollas M, Aguilar-Davidov B, Culebro-Garcia C, et al. (2012) Pathological implications of areas of lower enhancement on contrast-enhanced computed tomography in renal cell carcinoma: additional information for selecting candidates for surveillance protocols. Int Urol Nephrol 44:1369–1374
21. Yuan Q, Kapur P, Zhang Y (2016) Intratumor heterogeneity of perfusion and diffusion in clear-cell renal cell carcinoma: correlation with tumor cellularity. Clin Genitourin Cancer 14(6):e585–e594
22. Vargas H, Delany H, Delappe E, et al. (2013) Multiphasic contrast-enhanced MRI: single-slice versus volumetric quantification of tumor enhancement for assessment of renal clear-cell carcinoma fuhrman grade. J Magn Reson Imaging 37:1160–1167
23. Frank I, Blute ML, Cheville JC, et al. (2002) An outcome prediction model for patients with clear cell renal cell carcinoma treated with radical nephrectomy based on tumor stage, size, grade and necrosis: the SSIGN score. J Urol 168(6):2395–2400
24. Leibovich BC, Blute ML, Cheville JC, et al. (2003) Prediction of progression after radical nephrectomy for patients with clear cell renal cell carcinoma: a stratification tool for prospective clinical trials. Cancer 97(7):1663–1671
25. Sahni VA, Silverman SG (2014) Imaging management of incidentally detected small renal masses. Semin Interv Radiol 31(1):9–19
26. Coy H, Young JR, Douek M, et al. (2017) Quantitative computer-aided diagnostic algorithm for automated detection of peak lesion attenuation in differentiating clear cell from papillary and chromophobe renal cell carcinoma, oncocytoma, and fat-poor angiomyolipoma on multiphasic multidetector computed tomography. Abdom Radiol 42(7):1919–1928
27. Zhu YH, Wang X, Zhang J, et al. (2014) Low enhancement on multiphase contrast-enhanced CT images: an independent predictor of the presence of high grade tumor of clear cell renal cell carcinoma. Am J Roentgenol 203:W295–W300
28. Huhdanpaa H, Hwang D, Cen S, et al. (2015) CT prediction of the Fuhrman grade of clear cell renal cell carcinoma (RCC): towards the development of computer-assisted diagnostic method. Abdom Imaging 40(8):3168–3174
29. Kopp RP, Aganovic L, Palazzi KL, et al. (2013) Differentiation of clear from non-clear cell renal cell carcinoma using CT washout formula. Can J Urol 20(3):6790–6797
30. Sun M, Lughezani G, Jeldres C, et al. (2009) A proposal for reclassification of the Fuhrman grading system in patients with clear cell renal cell carcinoma. Eur Urol 56:775–781
31. Oh S, Sung DJ, Yang KS, et al. (2017) Correlation of CT imaging features and tumor size with Fuhrman grade of clear cell renal cell carcinoma. Acta Radiol 58(3):376–384
32. Frank I, Blute ML, Cheville JC, et al. (2002) An outcome prediction model for patients with clear cell renal cell carcinoma treated with radical nephrectomy based on tumor stage, size, grade and necrosis: the SSIGN score. J Urol 168:2395–2400
33. Vargas H, Delany H, Delappe E, et al. (2013) Multiphasic contrast-enhanced MRI: single-slice versus volumetric quantification of tumor enhancement for assessment of renal clear-cell carcinoma Fuhrman grade. J Magn Reson Imaging 37:1160–1167